Quantum interference in a lambda system driven by non-overlapping pulses with the same carrier frequency

James M. Supplee

Department of Physics, Drew University, Madison, New Jersey 07940, USA and Department of Physics and Engineering Physics, Stevens Institute of Technology, Hoboken, New Jersey 07030, USA (jsupplee@drew.edu)

Received February 18, 2010; revised May 3, 2010; accepted May 26, 2010;
posted June 3, 2010 (Doc. ID 124418); published July 13, 2010

This article describes quantum interference in a lambda system driven by two identical pulses that are each sufficiently broadband to drive both dipole-allowed transitions. The first pulse drives the system into a quantum superposition, making the effect of the second pulse depend critically on its optical phase and resulting in Ramsey-like fringes. This method, using just two pulses of the *same carrier frequency*, is conceptually simpler than in previous Raman–Ramsey studies, which use pump and Stokes pulses in each of two spatially separated regions. The goal here is not efficient population transfer, but to investigate narrow features resulting from quantum interference. I first explore these effects for low-inversion, which illustrates many key features using an easy-to-visualize model. I then use Schrödinger's equation in a semiclassical model to extend the results to arbitrary inversion. Informative quantum interference features remain when using this simplified scheme.

OCIS codes: 020.1670, 190.5650, 300.6450.

1. INTRODUCTION

Ramsey-fringe techniques [1–3] have a long and important history, including applications to time and frequency standards [4–14] and spectroscopy [15–23]. An important subset of the literature addresses quantum interference effects, including Ramsey-like fringes, in the case of *three-level* systems [6,7,17,24–36]. Ramsey-type work, in which a three-level Λ system is driven from one lower state to the other via a stimulated Raman transition, is sometimes aptly called "Raman–Ramsey" work. Interference effects in three-level systems driven by pulse pairs also have applications in coherent control [37,38] and for selecting a narrow velocity distribution of atoms [39,40]. There are calculations addressing the interaction of a three-level system with a quantized field (e.g., [26,41,42]). A subset of this work, e.g., in [32,35,36], involves driving the system into a dark state; the advantages of such schemes are discussed therein.

With many variations possible, an archetypical stimulated Raman–Ramsey setup can be pictured as a beam of three-level Λ atoms or molecules sent through two interaction regions. In each interaction region, the Λ system interacts with a pump and a Stokes electromagnetic field. In zone one, the Λ system is driven into a coherent superposition state. The later interaction, in zone two, depends sensitively on the phase relation between the driving fields in zone two and the quantum phase of the Λ system, which precessed freely between the zones. The physical reasons for this phase sensitivity are fundamentally similar to the case of traditional Ramsey fringes in a two-level system, as discovered in the Nobel Prize winning work of Ramsey [1,3].

This article uses a straightforward semiclassical model to study a case that is different from the cases studied in the work cited above: it explores the quantum interference structure that results from a *simplified technique using just one pulse, of one carrier frequency*, in each interaction region instead of using pump and Stokes beams. The amplitude and duration of the pulses are the same in each interaction region. The pulses are modeled as perfectly coherent pulses with a single carrier frequency and square envelopes. They are not few-cycle or "ultrashort" pulses, but are short enough to have sufficient bandwidth to drive both dipole-allowed transitions. Although the calculations below scale, a good exemplar case is the "optical Ramsey" case, with optical dipole-allowed transitions and with hyperfine splitting between the two lower states. The results below (i) show that a Ramsey-like fringe structure is still present and (ii) explore how the fringe structure changes as the relevant parameters change.

2. MODEL

Figure 1 shows the system of interest: a Λ system with energy levels $\epsilon_i=\hbar\omega_i$ $(i=1,2,3)$, where the lowest level is chosen to have $\epsilon_1=0$. In frequency units, the separation between the lower levels is

$$\delta \equiv \omega_3 - \omega_1 = \omega_3. \tag{1}$$

The Λ system is driven by an optical beam having carrier frequency ω. The overall detuning Δ, as shown in Fig. 1, is

$$\Delta \equiv \omega_0 - \omega, \tag{2}$$

where ω_0 is the average resonant frequency;

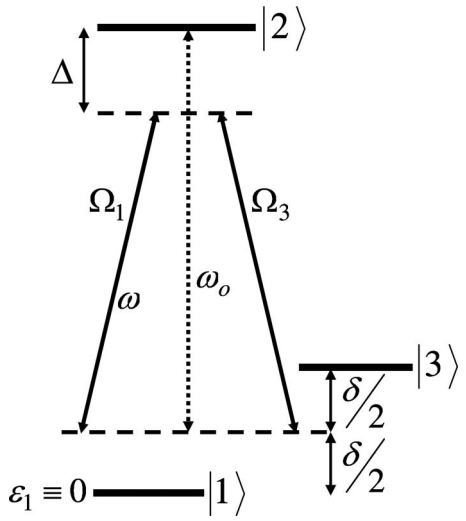

Fig. 1. "Resonant" frequency ω_o is defined as the energy difference (in frequency units) measured from the upper level to midway between the lower levels. The detuning is $\Delta \equiv \omega_o - \omega$. The figure is drawn with $\Delta > 0$.

$$\omega_0 \equiv \omega_2 - \frac{\omega_1 + \omega_3}{2} = \omega_2 - \frac{\omega_3}{2}; \tag{3}$$

the last equality follows because ω_1 is taken to be zero here. The single-photon detuning of the $|1\rangle$-$|2\rangle$ transition is

$$\Delta_1 \equiv \omega_2 - \omega = \Delta + \frac{\delta}{2}. \tag{4}$$

The last equality in Eq. (4) follows immediately from Fig. 1. Δ_3 is defined analogously to Δ_1; it is the detuning of the $|2\rangle$-$|3\rangle$ transition from single-photon resonance:

$$\Delta_3 \equiv \omega_2 - \omega_3 - \omega = \Delta - \frac{\delta}{2}. \tag{5}$$

Traditionally, the stimulated Raman–Ramsey effect involves a pump beam, generally nearly resonant with the dipole-allowed $|1\rangle$-$|2\rangle$ transition, and a Stokes beam, generally nearly resonant with the dipole-allowed $|2\rangle$-$|3\rangle$ transition. In this article, however, I consider only one carrier frequency ω. It is worth noting that with only one carrier frequency, the system is *never on two-photon resonance*; it is always detuned by the $|3\rangle$-$|1\rangle$ splitting δ. From an energy point of view, one might say that energy is conserved because the pulse bandwidth allows the energy absorbed by the $|1\rangle$-$|2\rangle$ transition to be slightly more than the energy emitted into the pulse by the $|2\rangle$-$|3\rangle$ transition.

This article addresses the response of a Λ system (called an "atom" for convenience) to two optically coherent pulses. The pulses are modeled as having square envelopes. For discussing the quantum interference due to two pulses, we can imagine atoms passing through two interaction zones, or atoms passing through one interaction zone twice, or two consecutive pulses hitting an atomic sample. Depending on the experimental details, the pulses can hit the atom with a zero or with a non-zero phase shift, as illustrated in Figs. 2(a) and 2(b), respectively. Case (a) might, for example, be obtained by pulsed amplification of a coherent cw laser. Case (b), with a stable but non-zero phase shift, could be obtained by splitting a pulse and sending one copy through an optical delay line. For case (b) a very small change in T (say by a fraction of an optical cycle) causes a change in the optical phase of the second pulse [16]. Therefore, case (b) requires controlling T with interferometric precision, as was done, for example, by Scherer *et al.* [43]. With a stable phase relation, quantum interference can result in either case, and the distinction between cases (a) and (b) has often been discussed, e.g., in [16,35,44–46]. For convenience and tractability, this article takes the phase shift as zero, using

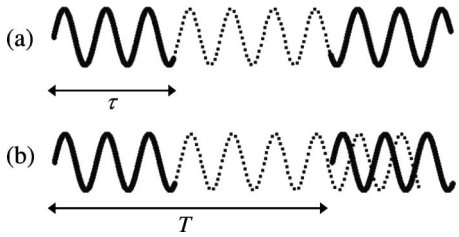

Fig. 2. (a) The two pulses are different parts of the same sinusoid. This could, for example, be obtained by pulsed amplification of a stable cw laser. (b) The second pulse is a time-delayed copy of the first pulse. Unless T is an integer multiple of the optical period, the second pulse will not be in phase with a mathematical continuation (shown dotted) of the first pulse. In both (a) and (b), τ is the duration of each pulse, and T is the time from the beginning of the first pulse to the beginning of the second pulse.

$$E(t) = f(t)\cos(\omega t), \tag{6}$$

where

$$f(t) = \begin{cases} E_0 & 0 \leq t \leq \tau \text{ and } T \leq t \leq T + \tau \\ 0 & \text{otherwise} \end{cases}. \tag{7}$$

E_0 is real here, because the absolute phase of the driving field is not critical. The overall phase represented by a complex E_0 would be significant if the envelope were only a few optical cycles or less in duration [46]. In this article, however, the critical phase of interest is the phase relation between the second pulse and the oscillating dipole moments. That phase is most directly controlled by T and the detunings, not by any overall phase contained in E_0.

3. EQUATIONS

This section gives the equations of motion for the probability amplitudes in the Schrödinger picture. The solutions to these equations will be plotted in Sections 4 and 5 to explore the behavior of the system under various conditions. The basis states are the energy eigenstates of the bare atom: $|j\rangle$, $(j = 1, 2, 3)$. So we have

$$\hat{H}_0|j\rangle = \epsilon_j|j\rangle, \tag{8}$$

where $\hat{H}_0$ is the Hamiltonian of the unperturbed atom and ϵ_j is the energy of state $|j\rangle$. An atomic superposition state can be written

$$|\Psi\rangle = C_1(t)e^{-i\Delta_1 t}|1\rangle + C_2(t)e^{-i\omega_2 t}|2\rangle + C_3(t)e^{-i\Delta_1 t}|3\rangle. \quad (9)$$

This phase choice results in constant coefficients in the coupled differential equations (below) for the C's when the laser is on.

The time development of the atomic state is given by Schrödinger's equation,

$$\frac{\mathrm{d}}{\mathrm{d}t}|\Psi\rangle = -\frac{i}{\hbar}[\hat{H}_0 + \hat{V}(t)]|\Psi\rangle, \quad (10)$$

where $\hat{V}(t)$ is the interaction Hamiltonian. Approximating $\hat{V}(t)$ using the customary dipole approximation [47,48] gives

$$V_{ij} = -q_e\langle i|\hat{x}|j\rangle f(t)\cos(\omega t) = \hbar\Omega_{ij}(t)\cos(\omega t). \quad (11)$$

Here $q_e\hat{x}$ is the atomic dipole moment expectation value operator projected onto the axis of the optical field polarization. $\Omega_{ij}(t) \equiv -q_e\langle i|\hat{x}|j\rangle f(t)/\hbar$ is the usual Rabi frequency, representing the interaction energy in frequency units. The only non-zero matrix elements V_{ij} are for the dipole allowed transitions: $V_{12}=V_{21}^*$ and $V_{23}=V_{32}^*$. This allows for a slight simplification in notation as shown in Fig. 1: $\Omega_{12}\rightarrow\Omega_1$ and $\Omega_{23}\rightarrow\Omega_3$. For convenience, I take the Ω_i as real. (See, e.g., [49], pp. 780, 781.)

Using the wave function, Eq. (9), in the Schrödinger Eq. (10) gives the differential equation for the time evolution of the C's:

$$\begin{aligned}(\dot{C}_1 - i\Delta_1 C_1)e^{-i\Delta_1 t}|1\rangle + (\dot{C}_2 - i\omega_2 C_2)e^{-i\omega_2 t}|2\rangle \\ + (\dot{C}_3 - i\Delta_1 C_3)e^{-i\Delta_1 t}|3\rangle \\ = -\frac{i}{\hbar}[VC_1e^{-i\Delta_1 t}|1\rangle + (\epsilon_2 + V)C_2e^{-i\omega_2 t}|2\rangle \\ + (\epsilon_3 + V)C_3e^{-i\Delta_1 t}|3\rangle]. \quad (12)\end{aligned}$$

Using the usual techniques [47–50], including the rotating wave approximation and the dipole approximation, the time evolution of the C's can be extracted from Eq. (12) and is

$$\dot{C}_1 = \frac{i}{2}(2\Delta_1 C_1 - \Omega_1 C_2); \quad (13)$$

$$\dot{C}_2 = -\frac{i}{2}(\Omega_1^* C_1 + \Omega_3 C_3); \quad (14)$$

$$\dot{C}_3 = -\frac{i}{2}(\Omega_3^* C_2 - \Delta_3 C_3). \quad (15)$$

The simplicity of these equations is the result of the approximations mentioned just above and also because $V_{11}=V_{22}=V_{33}=V_{13}=0$.

Writing Eqs. (13)–(15) together in matrix form yields

$$\frac{\mathrm{d}}{\mathrm{d}t}\mathbf{C} = -\frac{i}{2}\mathbf{M}\mathbf{C}, \quad (16)$$

where $\mathbf{C} \equiv [C_1, C_2, C_3]^{\mathrm{T}}$, and

$$\mathbf{M} \equiv \begin{bmatrix} -2\Delta_1 & \Omega_1(t) & 0 \\ \Omega_1^*(t) & -i\gamma & \Omega_3(t) \\ 0 & \Omega_3^*(t) & -2\Delta_3 \end{bmatrix}. \quad (17)$$

The $i\gamma$ term has been appended to allow for relaxation of the upper state out of the system.

4. SHORT, WEAK PULSE LIMIT

A. Solution

The case of short, weak pulses ($\tau \ll 1/\Delta_i$ and low inversion) allows for conceptual and mathematical simplification, which facilitates checking some fundamentals. The results in this section are consistent with intuition carried over from traditional Raman–Ramsey studies (using pump and Stokes beams), and also somewhat resemble the simpler case of Ramsey fringes in a two-level system. Good agreement between Sections 4 and 5 also shows that the intuition developed in Section 4 can facilitate understanding of the more formal and general results in Section 5.

Consider (throughout this article) an atom starting in the lowest state $|1\rangle$. An optical pulse then drives the atom into a superposition state. In the "weak pulse limit" (this section), the first pulse will leave most of the population in state $|1\rangle$. Some of the population will be driven to state $|2\rangle$, and a small fraction to state $|3\rangle$. But what about the second pulse? A reasonable guess is that the second pulse will drive more population along this two-step path (that is, will cause constructive interference) if the second pulse is in phase with the already oscillating dipoles. By the definition of detunings, the driving field ω drifts out of phase with the freely oscillating $|1\rangle$-$|2\rangle$ and $|2\rangle$-$|3\rangle$ dipoles at a rate given by the detunings Δ_1 and Δ_3. If the field drifts out of phase by a whole number of cycles, then it is back in phase. That is, the second pulse will arrive in phase with each oscillating dipole transition if

$$\Delta_1 T = 2n\pi \quad (18)$$

and

$$\Delta_3 T = 2m\pi, \quad (19)$$

where n and m are integers. (These pulse delay conditions have a similar significance [51] in frequency comb calculations.) If the pulse is to be in phase with both oscillations, then the oscillations must be in phase with each other. That is, the $|1\rangle$-$|2\rangle$ oscillation and the $|2\rangle$-$|3\rangle$ oscillation should have drifted out of phase by $2p\pi$ where p is an integer:

$$(\omega_2 - \omega_1)T - (\omega_2 - \omega_3)T = \omega_3 T \equiv \delta T = 2p\pi. \quad (20)$$

Put differently, Eq. (20) can also be obtained by simply subtracting Eq. (19) from Eq. (18).

Equations (18)–(20) can be supported further by solving Eq. (16). For simplicity in the examples below, consider the Rabi frequencies to be equal:

$$\Omega_1(t) = \Omega_3(t) = \begin{cases} \Omega, & \text{pulse on} \\ 0, & \text{pulse off} \end{cases}. \tag{21}$$

For a weak pulse, most of the population will remain in state $|1\rangle$. A small fraction of the population will be driven to state $|2\rangle$ and a still smaller fraction to state $|3\rangle$. That is,

$$|C_1| \approx 1 \text{ and } |C_3| \ll |C_2| \ll 1. \tag{22}$$

These approximations simplify the differential equations for the C's, Eqs. (13)–(15). Neglecting C_2 compared to C_1, Eq. (13) for C_1 integrates to

$$C_1 = e^{i\Delta_1 t}. \tag{23}$$

Moving on to C_2: neglecting decay ($\gamma \approx 0$), neglecting C_3 compared to C_1, and using Eq. (23), Eq. (14) becomes

$$\dot{C}_2 \approx \begin{cases} -\frac{i}{2}\Omega e^{i\Delta_1 t}, & \text{pulse on} \\ 0, & \text{pulse off} \end{cases}. \tag{24}$$

Similarly, Eq. (15) for C_3 simplifies to

$$\dot{C}_3 \approx \begin{cases} -\frac{i}{2}\Omega C_2, & \text{pulse on} \\ i\Delta_3 C_3, & \text{pulse off} \end{cases}. \tag{25}$$

The "pulse-off" part is taken exactly from Eq. (15), while the "pulse-on" part has been simplified by dropping the C_3 term because it is assumed small compared with the C_2 term.

The approximate solutions to Eqs. (24) and (25) are

$$C_2 \approx \begin{cases} -\frac{i\Omega}{2}t, & 0 \le t \le \tau \\ -\frac{i\Omega}{2}\tau, & \tau \le t \le T \\ -\frac{i\Omega}{2}[\tau + (t-T)e^{i\Delta_1 T}], & T \le t \le T+\tau \end{cases}; \tag{26}$$

$$C_3 \approx \begin{cases} -\frac{\Omega^2}{8}t^2, & 0 \le t \le \tau \\ -\frac{\Omega^2}{8}\tau^2 e^{i\Delta_3 t}, & \tau \le t \le T \\ -\frac{\Omega^2}{8}[2\tau(t-T) + (t-T)^2 e^{i\Delta_1 T} + \tau^2 e^{i\Delta_3 T}], & T \le t \le T+\tau \end{cases}. \tag{27}$$

Eqs. (26) and (27) come from integrating Eqs. (24) and (25) three times: for the first pulse, for the dark time between pulses, and for the second pulse. The integration constants make the C's continuous at the boundaries. I also used the "short-pulse" approximation

$$\tau \ll 1/\Delta_i \quad \text{(in this section)}, \tag{28}$$

by using $e^{i\Delta_i \tau} \approx 1$. In words: the assumption in this section (unlike Section 5) is that the pulse bandwidth is much greater than the detunings. This is the physical reason why some expressions above are insensitive to the detunings; for example, there is no detuning in the expressions for C_2 or C_3 at the end of the first pulse. Detuning insensitivity when using a single broadband pulse is a standard textbook result; e.g., the top line of Eq. (26) matches Eq. (2.8.14) of [48].

The final value of C_3 is given by evaluating Eq. (27) at $t = T + \tau$, yielding

$$C_3^f \approx -\frac{\Omega^2}{8}\tau^2(2 + e^{i\Delta_1 T} + e^{i\Delta_3 T}). \tag{29}$$

The final population in state $|3\rangle$ is given by

$$P_3 = |C_3^f|^2 \approx \frac{\Omega^4}{64}\tau^4(2 + e^{i\Delta_1 T} + e^{i\Delta_3 T})(2 + e^{-i\Delta_1 T} + e^{-i\Delta_3 T})$$
$$= \frac{\Omega^4\tau^4}{32}(3 + 2\cos\Delta_1 T + 2\cos\Delta_3 T + \cos\delta T). \tag{30}$$

Equation (30) agrees with the intuitive results in Eqs. (18)–(20) above: the population will be largest when the three cosines in Eq. (30) are near 1.

Using Eqs. (4) and (5) allows rewriting Eq. (30) in terms of the overall detuning Δ as

$$P_3 = \frac{\Omega^4\tau^4}{32}\left(3 + \cos\delta T + 4\cos\Delta T\cos\frac{\delta T}{2}\right). \tag{31}$$

Figure 3 shows P_3 versus Δ for three different values of T. (Reassuringly, a plot for the same parameters made using the more formal results of Section 5 is indistinguishable from Fig. 3.) Because the variable Δ appears just once in Eq. (31), the curves for various T are simply scaled and shifted cosines. For both the heavy solid curve and the dashed curve in Fig. 3, T is chosen so that $\cos(\delta T/2) = 1$.

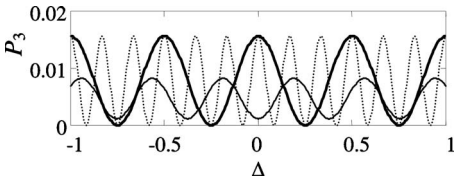

Fig. 3. Final population in state $|3\rangle$ as a function of detuning Δ. All curves have $\Omega=10$ and $\tau=0.05$ in units chosen so that $\delta=1$. The heavy solid curve has $T=4\pi$; the dashed curve has $T=12\pi$; the light solid curve has $T=5.3\pi$ (to illustrate a non-integer multiple of π). As is typical with Ramsey fringes, the fringe width is of order $1/T$. In contrast, a single pulse of duration $\tau=0.05$ would result in a peak much broader than the entire figure.

Therefore, the term in parentheses varies from zero to 8. The FWHM of each fringe is π/T. The dashed curve has T three times as long as the heavy solid curve, so the fringes are one-third as wide. All of the fringes in Fig. 3 are much narrower than the bandwidth of a single pulse, which is of order $1/\tau$. ($1/\tau$ equals 20 in the units of Fig. 3.) Having fringe width governed by $1/T$ rather than $1/\tau$ is a hallmark of traditional Ramsey fringes; Fig. 3 shows that this crucial property carries over to the nontraditional case considered in this article.

The light solid curve in Fig. 3 illustrates how the product δT can affect the interference amplitude. In Eq. (31), the term $\cos(\delta T/2)$ multiplies the oscillating term and therefore sets the scale of the oscillation. Because that cosine can range between -1 and $+1$, the oscillation will scale and can change sign as T changes. The light solid curve shows a case with $\cos(\delta T/2)$ negative, so the oscillations are inverted. Also, because $\cos(\delta T/2)$ is not all the way to -1, that curve has smaller oscillations.

B. Frequency Domain Discussion

Equations (18)–(20) above, along with the basic structure of Fig. 3, are consistent with intuition about "in-phase timing" for constructive interference. For low inversion, the resonance structure can also be understood from the frequency domain point of view, which is widely used; see, e.g., [1,2,52,53].

Effectively picturing the frequency domain requires keeping in mind that the pulses are broadband. In the time domain, Fig. 2(a) might have tempted one to say simply that the second pulse is "in phase" with the first. However, each pulse has a frequency *spectrum*, and various frequency components will have various phase relations. The main issue is not necessarily whether the carrier frequency is in phase from pulse to pulse, but whether the frequency components matching the allowed transitions interfere constructively. This issue of pulse-to-pulse interference also arises for a similar reason in frequency-comb spectroscopy. (See, e.g., [9,22,23,51,54–56].) Frequency-comb work is in a different parameter regime than the one addressed here; it addresses the more extreme case of ultrashort coherent pulses. Because of their extreme bandwidth, ultrashort pulses can interfere constructively at many frequencies, hence giving rise to the "frequency comb." Although the parameter regime is different in that work and this, the phase delay concept is of similar importance. For example, [51] (p. 7) describes the pulse-to-pulse interference requirement in their case "by noting that for the laser modes to match both atomic transitions, then the difference between the atomic frequencies must be equal to some multiple of the mode spacing $2\pi/T$." That point of view agrees with Eq. (20) above. For this article, I will continue the discussion in the time domain, and now turn to the more general case, including arbitrary inversion.

5. GENERAL CASE, INCLUDING ARBITRARY INVERSION

A. General Solution

The approximate solution for the population in state $|3\rangle$, Eq. (31), is useful because it reveals the physics effectively; it explicitly displays how each parameter enters. Even when discussing the exact solution below, I will sometimes refer back to Eq. (31), because it can make the physics transparent.

To obtain a more general solution that holds for arbitrary inversion, we can directly integrate Eq. (16), giving the formal solution

$$\mathbf{C}(t)=e^{-\frac{i}{2}\mathbf{M}t}\mathbf{C}(0). \tag{32}$$

Equation (16) could also be addressed by finding the eigenvalues and eigenvectors of $\mathbf{M}$, but that algebra yielded no further physical insight, so I will leave the general solution written compactly as Eq. (32). For plotting the various cases below, I used a power series expansion of the exponential in Eq. (32), while keeping enough terms to insure that each plot represents the actual solution. The number of terms needed depends on the parameters.

Finding the final population in state $|3\rangle$ requires stepping through the "on-off-on" pulse sequence, much like in the previous section. $\mathbf{C}(\tau)$ is given by evaluating Eq. (32) at $t=\tau$, and with the atom starting in the ground state $\mathbf{C}^{\mathrm{T}}(0)=(1,0,0)$. The "pulse-off" part of the evolution is simple: putting both Rabi frequencies equal to 0 in $\mathbf{M}$ shows that the atom simply precesses and decays. Therefore at the end of the "off-time" we have

$$C_1(T)=e^{i\Delta_1(T-\tau)}C_1(\tau),$$

$$C_2(T)=e^{-\frac{\gamma}{2}(T-\tau)}C_2(\tau),$$

$$C_3(T)=e^{i\Delta_3(T-\tau)}C_3(\tau). \tag{33}$$

These coefficients become the initial conditions for the second pulse. The effect of the second pulse is calculated in the same way as for the first pulse: by using Eq. (32), but with the initial conditions appropriate for the second pulse,

$$\mathbf{C}^f=e^{-\frac{i}{2}\mathbf{M}\tau}\mathbf{C}(T). \tag{34}$$

The final upper-state population is

$$P_3=|C_3^f|^2. \tag{35}$$

B. Agreement in the Low Inversion Case

In any situation to which the assumptions of Section 4 apply, Eq. (31) and Eq. (35) agree. For example, for the three

curves plotted in Fig. 3, Eqs. (31) and (35) give indistinguishable results. The reason for presenting both equations is this: Eq. (35) applies more generally, because neither the low inversion approximation [Eqs. (22)] nor the short-pulse approximation [Eq. (28)] was used. However, the more restricted result, Eq. (31), is useful because it explicitly displays the parameter dependence, allowing for a more intuitive understanding of the physics.

C. Velocity Averaging

For the case of an atomic beam traveling through two interaction regions, different atoms have different speeds, and hence have different travel times; that is, different atoms have different T. This is a Doppler broadening effect that is considered disadvantageous in some circumstances, but in Ramsey experiments it offers the important *advantage* of identifying the main peak at $\Delta=0$. This advantage is important enough that averaging over T is often artificially introduced into two-pulse experiments with trapped atoms by using a range of optical pulse delays and then averaging the results (e.g., in [2,18,57,58]). The point of averaging over T in a two-pulse experiment using *two-level* atoms is this: the constructive interference peak with zero detuning remains, because a resonant drive stays resonant regardless of the dark time. However, constructive interference peaks due to a relative phase shift between pulses of 2π, 4π, 6π, etc., are washed out, because having *those* phase delays is T-dependent. Because the side peaks wash out, the central peak can be unambiguously identified. The results in this subsection show that for *three-level* atoms, averaging over T depends on the averaging interval in a more complex way.

A great deal can (and has) been said about the details of velocity averaging. The details depend on many factors, including whether the variation in T is due to a spread of atomic velocities in a beam or due to controlled variation of two pulses interacting with a sample of trapped atoms. This article does not address a myriad of averaging schemes; rather, it addresses two core issues: (1) Do the fringes remain after velocity averaging? (They do.) (2) How does changing the range of delay times T included in the averaging affect the signal?

The T averaged results shown as bold curves in Fig. 4 are obtained by a simple boxcar average,

$$P_3^{avg}(\Delta, T_{\max}, T_{\min}) = \frac{1}{T_{\max} - T_{\min}} \int_{T_{\min}}^{T_{\max}} P_3(\Delta, T')\mathrm{d}T'. \tag{36}$$

The bold curves in Figs. 4(a)–4(c) show a striking variation, which is due solely to their having different averaging limits. The progression in Fig. 4 can be understood with the help of Eq. (31) (even thought the more precise results of Section 5 were used to make these graphs). The not-velocity-averaged (dashed) curves in Fig. 4 are fundamentally the result of the $\cos \Delta T$ term in Eq. (31). As mentioned earlier in connection with two-level systems, this term is positive when $\Delta=0$ regardless of T. That is why the $\Delta=0$ peak does not wash out in the averaging for a *two-level* atom. However, some additional complexity of a three-level atom is revealed by the $\cos(\delta T/2)$ term that multiplies $\cos \Delta T$ in Eq. (31). The $\cos(\delta T/2)$ term changes

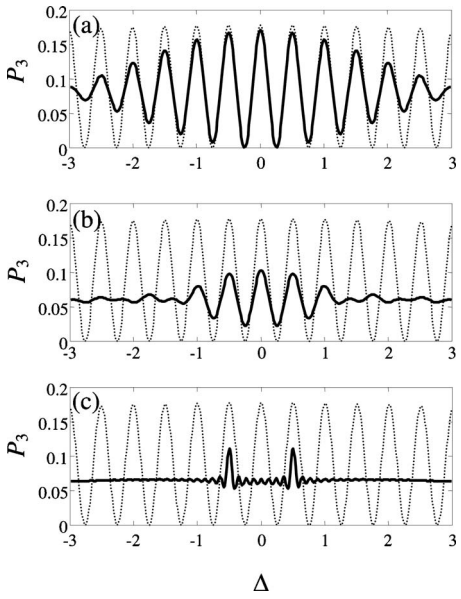

Fig. 4. The only change among the three graphs is the velocity averaging interval. All three graphs have $\Omega=5$ and $\tau=0.2$ in units chosen so that $\delta=1$. For comparison, the dashed curves show the non-velocity-averaged population in state $|3\rangle$ as a function of detuning for a pulse delay of $T=4\pi$. The solid curves show the result when averaged using Eq. (36). (a) Averages over $T=4\pi\pm1$. (b) Averages over $T=4\pi\pm4$. (c) Averages from $T=4\pi-10$ to $4\pi+40$. The purpose of the asymmetric averaging interval in (c) is simply to allow a very large range of T without going below τ, which would be unphysical. The striking qualitative change is discussed in the text.

sign if T is varied greatly, eventually causing the $\Delta=0$ peak to wash out. Figure 4 shows an example of such a progression. In Fig. 4(a), the range of velocity integration is $T=4\pi\pm1$, in units with $\delta=1$. The purpose of this choice is to keep $\cos(\delta T/2)$ always positive. This makes the last term in Eq. (31), evaluated at $\Delta=0$, $4\times1\times$(a positive). Averaging over just positive numbers retains the peak at $\Delta=0$. In Fig. 4(b), the solid curve is averaged over $T=4\pi\pm4$, which includes some negative values of $\cos(\delta T/2)$, thereby reducing the height of the main peak. This broader range of T is sufficiently large that the *noncentral* peaks are averaged over enough positive and negative values to wash out. This is a hallmark of the effect of velocity averaging in Ramsey fringes.

Figure 4(c) uses an even broader range of T in averaging, and reveals an effect with no exact equivalent in Ramsey fringes for two-level systems. Figure 4(c) can be thought of algebraically or physically. In algebraic terms, the product of cosines in Eq. (31) will include both positive and negative numbers, and will therefore average to near zero if an extremely wide range of T is sampled. The exception to that is when $\Delta=\pm\delta/2$; for that case, the last term in Eq. (31) is a cosine squared term, and will therefore never average to zero. In physical terms, $\Delta=\pm\delta/2$ is where the carrier is resonant with one of the dipole-allowed transitions, as shown by Eqs. (4) and (5). Hence, the peaks at $\Delta=\pm1/2$ (in units where $\delta=1$) in Fig. 4(c) show the allowed transition frequencies. This is an interesting shift—from identifying the central fringe at $\Delta=0$, to identifying the two dipole-allowed resonances.

Figure 5(a) further illustrates how Eq. (31) can afford some simple understanding of population inversion. First,

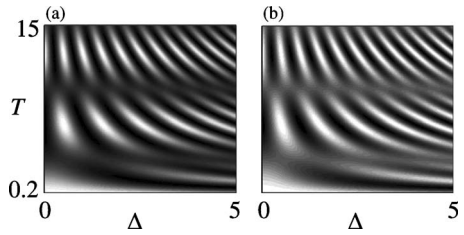

Fig. 5. (a) Population in state $|3\rangle$ versus detuning Δ and pulse delay time T. Units are chosen so that $\delta=1$. The other parameters are $\tau=0.2$, $\Omega=7$, and $\gamma=0$. The maximum population is 0.49 and is indicated by white; black indicates no population in $|3\rangle$. (b) White indicates places where one would have expected high inversion from the extremely naïve guess based on Eqs. (18) and (19). The agreement is quite good, considering that the naïve guess should become less and less reliable as inversion increases.

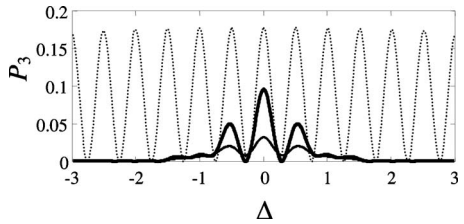

Fig. 6. The dashed curve is identical to those in Fig. 4, again having $T=4\pi$, $\Omega=5$, and $\tau=0.2$ in units chosen so that $\delta=1$. The heavy solid curve has $\tau=4$, giving the pulse a narrower bandwidth and hence identifying the central peak. The pulse area is the same in both cases, with $\Omega\tau=1$. The lighter solid curve confirms that decay ($\gamma=0.2$) simply lowers the overall signal. There is no velocity averaging in this figure.

since the important $\cos(\Delta T)$ term contains Δ and T only as a product, the graph shows basically hyperbolic contours, because the product is constant along hyperbolas. Second, Eq. (31) clearly reveals why the contours flip from black to white along horizontal bands at $T=\pi$ and 3π. This is because the $\cos(\Delta T)$ term causing the hyperbolas is multiplied by $\cos(\delta T/2)$, which changes sign at $T=\pi$ and 3π.

Comparing Figs. 5(a) and 5(b) shows that using Eqs. (18) and (19) to get a good sense of inversion is justified even for nontrivial inversion. Figure 5(a) shows the actual inversion as a function of Δ and T, while Fig. 5(b) shows where one might have casually guessed inversion would be large. The guess in Fig. 5(b) is simply a plot of $\cos(\Delta_1 T)+\cos(\Delta_3 T)$, chosen because that expression gives a crude map of where Eqs. (18) and (19) are true. More precisely, $\cos(\Delta_1 T)+\cos(\Delta_3 T)$ is contained in the middle term in Eq. (30), which reveals the same physics.

D. Longer Pulses

There is another way (besides averaging over T) to identify the central interference peak. Figure 6 illustrates this. The dashed curve in Fig. 6 is identical to the dashed curves in Fig. 4. The heavy solid curve in Fig. 6 shows the effect of increasing τ. There is no velocity averaging whatsoever in Fig. 6; rather, increasing τ simply gives the pulses a narrower bandwidth and identifies the central peak. The lighter solid curve in Fig. 6 shows that decay ($\gamma\neq 0$) has the expected effect of lowering the signal.

6. CONCLUSIONS

A pulse of sufficient bandwidth can drive both dipole-allowed transitions in a Λ system. Two optically-coherent pulses can cause quantum interference effects: the first pulse leaves the atom in a superposition state, and the effect of the second pulse depends critically on its phase relation with the already-excited system. This article demonstrates that such stimulated Raman–Ramsey quantum interference effects can be studied in a simplified manner—using a total of just two pulses of one carrier frequency, rather than using the traditional pump and Stokes fields in each interaction. The physics underlying the resulting quantum interference effects has been explored and illustrated in detail here using a straightforward semiclassical model.

ACKNOWLEDGMENTS

Drew University and Stevens Institute of Technology provided support for this research. I appreciate Marty Ligare, Robert Murawski, and Chris Search making insightful comments on a draft of this article. Paul Berman, Wally Buell, Dan Gauthier, A. "Kumar" Kumarakrishnan, Rainer Martini, Ron Walsworth, Ed Whittaker, and two reviewers also made very helpful suggestions.

REFERENCES

1. N. F. Ramsey, *Molecular Beams* (Oxford Univ. Press, 1956), Section V.4.
2. Ye. V. Baklanov, B. Ya. Dubetsky, and V. P. Chebotayev, "Non-linear Ramsey resonance in the optical region," Appl. Phys. **9**, 171–173 (1976).
3. N. F. Ramsey, "Experiments with separated oscillatory fields and hydrogen masers," Rev. Mod. Phys. **62**, 541–552 (1990).
4. J. Vanier and C. Audoin, *The Quantum Physics of Atomic Frequency Standards* (IOP Publishing, 1989).
5. F. G. Major, *The Quantum Beat—The Physical Principles of Atomic Clocks* (Springer, 1998).
6. Walter F. Buell, "Laser-pumped and laser-cooled atomic clocks for space applications," Laser Part. Beams **16**, 627–639 (1998).
7. A. Godone, S. Micalizio, and F. Levi, "Pulsed optically pumped frequency standard," Phys. Rev. A **70**, 023409 (2004).
8. V. Letchumanan, P. Gill, E. Riis, and A. G. Sinclair, "Optical Ramsey spectroscopy of a single trapped $^{88}Sr^{+}$ ion," Phys. Rev. A **70**, 033419 (2004).
9. A. Shelkovnikov, C. Grain, R. J. Butcher, A. Amy-Klein, A. Goncharov, and C. Chardonnet, "Two-Photon Ramsey Fringes at 30 THz Referenced to an H Maser/Cs Fountain via an Optical-Frequency Comb at the 1-Hz Level," IEEE J. Quantum Electron. **40**, 1023–1029 (2004).
10. S. Bize, P. Laurent, M. Abgrall, H. Marion, I. Maksimovic, L. Cacciapuoti, J. Grünert, C. Vian, F. Pereira dos Santos, P. Rosenbusch, P. Lemonde, G. Santarelli, P. Wolf, A. Clairon, A. Luiten, M. Tobar, and C. Salomon, "Cold atom clocks and applications," J. Phys. B **38**, S449–S468 (2005).
11. V. Letchumanan, P. Gill, A. G. Sinclair, and E. Riis, "Optical-clock local-oscillator stabilization scheme," J. Opt. Soc. Am. B **23**, 714–717 (2006).
12. S. T. Müller, D. V. Magalhães, A. Bebeachibuli, T. A. Ortega, M. Ahmed, and V. S. Bagnato, "Free expanding cloud of cold atoms as an atomic standard: Ramsey fringes contrast," J. Opt. Soc. Am. B **25**, 909–914 (2008).
13. E. A. Curtis, C. W. Oates, and L. Hollberg, "Quenched

narrow-line second- and third-stage laser cooling of ^{40}Ca," J. Opt. Soc. Am. B **20**, 977–984 (2003).
14. J. J. McFerran and A. N. Luiten, "Fractional frequency instability in the 10^{-14} range with a thermal beam optical frequency reference," J. Opt. Soc. Am. B **27**, 277–285 (2010).
15. Ye. V. Baklanov, V. P. Chebotayev, and B. Ya Dubetsky, "The resonance of two-photon absorption in separated optical fields," Appl. Phys. **11**, 201–202 (1976).
16. M. M. Salour, "Quantum interference effects in two-photon spectroscopy," Rev. Mod. Phys. **50**, 667–681 (1978).
17. R. E. Tench, B. W. Peuse, P. R. Hemmer, J. E. Thomas, S. Ezekiel, C. C. Leiby Jr., R. H. Picard, and C. R. Willis, "Two laser Raman difference technique applied to high precision spectroscopy," J. Phys. (Paris) **42**, C8–45 (1981).
18. L. S. Vasilenko, I. D. Matveyenko, and N. N. Rubtsova, "Study of narrow resonances of coherent radiation in time separated fields in SF_6," Opt. Commun. **53**, 371–374 (1985).
19. B. Gross, A. Huber, M. Niering, M. Weitz, and T. W. Hänsch, "Optical Ramsey spectroscopy of atomic hydrogen," Europhys. Lett. **44**, 186–191 (1998).
20. L. Marmet and A. A. Madej, "Optical Ramsey spectroscopy and coherence measurements of the clock transition in a single trapped Sr ion," Can. J. Phys. **78**, 495–507 (2000).
21. M. Bellini, S. Cavalieri, C. Corsi, R. Eramo, and M. Materazzi, "Mutually coherent high-order harmonic pulses for XUV Ramsey spectroscopy," Laser Phys. **15**, 324–327 (2005).
22. S. Witte, R. Th. Zinkstok, W. Ubachs, W. Hogervorst, and K. S. E. Eikema, "Deep-ultraviolet quantum interference metrology with ultrashort laser pulses," Science **307**, 400–403 (2005).
23. R. Th. Zinkstok, S. Witte, W. Ubachs, W. Hogervorst, and K. S. E. Eikema, "Frequency comb laser spectroscopy in the vacuum-ultraviolet region," Phys. Rev. A **73**, 061801(R) (2006).
24. J. E. Thomas, P. R. Hemmer, S. Ezekiel, C. C. Leiby Jr., R. H. Picard, and C. R. Willis, "Observation of Ramsey fringes using a stimulated, resonance Raman transition in a sodium atomic beam," Phys. Rev. Lett. **48**, 867–870 (1982).
25. P. R. Hemmer, G. P. Ontai, and S. Ezekiel, "Precision studies of stimulated-resonance Raman interactions in an atomic beam," J. Opt. Soc. Am. B **3**, 219–230 (1986).
26. B. J. Dalton, T. D. Kieu, and P. L. Knight, "Theory of ultrahigh-resolution optical Raman Ramsey spectroscopy," Opt. Acta **33**, 459–472 (1986).
27. P. R. Hemmer and M. G. Prentiss, "Coupled-pendulum model of the stimulated resonance Raman effect," J. Opt. Soc. Am. B **5**, 1613–1623 (1988).
28. P. R. Hemmer, M. S. Shahriar, V. D. Natoli, and S. Ezekiel, "Ac Stark shifts in a two-zone Raman interaction," J. Opt. Soc. Am. B **6**, 1519–1528 (1989).
29. P. R. Hemmer, M. S. Shahriar, H. Lamela-Rivera, S. P. Smith, B. E. Bernacki, and S. Ezekiel, "Semiconductor laser excitation of Ramsey fringes by using a Raman transition in a cesium atomic beam," J. Opt. Soc. Am. B **10**, 1326–1329 (1993).
30. M. S. Shahriar, P. R. Hemmer, D. P. Katz, A. Lee, and M. G. Prentiss, "Dark-state-based three-element vector model for the stimulated Raman interaction," Phys. Rev. A **55**, 2272–2282 (1997).
31. A. S. Zibrov and A. B. Matsko, "Optical Ramsey fringes induced by Zeeman coherence," Phys. Rev. A **65**, 013814 (2001).
32. T. Zanon, S. Guerandel, E. de Clercq, D. Holleville, N. Dimarcq, and A. Clairon, "High contrast Ramsey fringes with coherent-population-trapping pulses in a double lambda atomic system," Phys. Rev. Lett. **94**, 193002 (2005).
33. Y. Xiao, I. Novikova, D. F. Phillips, and R. L. Walsworth, "Diffusion-induced Ramsey narrowing," Phys. Rev. Lett. **96**, 043601 (2006).
34. J. Vanier, "Atomic clocks based on coherent population trapping: a review," Appl. Phys. B **81**, 421–442 (2005).
35. G. S. Pati, K. Salit, R. Tripathi, and M. S. Shahriar, "Demonstration of Raman-Ramsey fringes using time delayed optical pulses in rubidium vapor," Opt. Commun. **281**, 4676–4680 (2008).
36. J. Fuchs, G. J. Duffy, W. J. Rowlands, and A. M. Akulshin, "Electromagnetically induced transparency in ^{6}Li," J. Phys. B **39**, 3479–3489 (2006).
37. D. Felinto, C. A. C. Bosco, L. H. Acioli, and S. S. Vianna, "Accumulative effects in temporal coherent control," Phys. Rev. A **64**, 063413 (2001).
38. R. Netz, A. Nazarkin, and R. Sauerbrey, "Observation of selectivity of coherent population transfer induced by optical interference," Phys. Rev. Lett. **90**, 063001 (2003).
39. K. Moler, D. S. Weiss, M. Kasevich, and S. Chu, "Theoretical analysis of velocity-selective Raman transitions," Phys. Rev. A **45**, 342–348 (1992).
40. M. Kasevich, D. S. Weiss, E. Riis, K. Moler, S. Kasapi, and S. Chu, "Atomic velocity selection using stimulated Raman transitions," Phys. Rev. Lett. **66**, 2297–2300 (1991).
41. H.-I. Yoo and J. H. Eberly, "Dynamical theory of an atom with two or three levels interacting with quantized cavity fields," Phys. Rep. **118**, 239–337 (1985).
42. S. Bougouffa and A. Kamli, "An analytic approach to a three-level atom interacting with a single-mode quantized field," J. Opt. B: Quantum Semiclassical Opt. **6**, S60–S65 (2004).
43. N. F. Scherer, R. J. Carlson, A. Matro, M. Du, A. J. Ruggiero, V. Romero-Rochin, J. A. Cina, G. R. Fleming, and S. A. Rice, "Fluorescence-detected wave packet interferometry: Time resolved molecular spectroscopy with sequences of femtosecond phase-locked pulses," J. Chem. Phys. **95**, 1487–1511 (1991).
44. M. M. Salour and C. Cohen-Tannoudji, "Observation of Ramsey's interference fringes in the profile of Doppler-free two-photon resonances," Phys. Rev. Lett. **38**, 757–760 (1977).
45. N. V. Vitanov and P. L. Knight, "Coherent excitation of a two-state system by a train of short pulses," Phys. Rev. A **52**, 2245–2261 (1995).
46. A. W. Albrecht, J. D. Hybl, S. M. G. Faeder, and D. M. Jonas, "Experimental distinction between phase shifts and time delays: Implications for femtosecond spectroscopy and coherent control of chemical reactions," J. Chem. Phys. **111**, 10934–10956 (1999).
47. P. Meystre and M. Sargent III, *Elements of Quantum Optics*, 3rd ed. (Springer, 1999).
48. R. Loudon, *The Quantum Theory of Light*, 3rd ed. (Oxford Univ. Press, 2000).
49. B. W. Shore, *The Theory of Coherent Atomic Excitation* (Wiley, 1990).
50. M. Sargent III, M. O. Scully, and W. E. Lamb Jr., *Laser Physics* (Westview, 1974).
51. D. Felinto, L. H. Acioli, and S. S. Vianna, "Accumulative effects in the coherence of three-level atoms excited by femtosecond-laser frequency combs," Phys. Rev. A **70**, 043403 (2004).
52. R. Teets, J. Eckstein, and T. W. Hänsch, "Coherent two-photon excitation by multiple light pulses," Phys. Rev. Lett. **38**, 760–764 (1977).
53. R. E. Carley, E. D. Boléat, R. S. Minns, R. Patel, and H. H. Fielding, "Interfering Rydberg wave packets in Na," J. Phys. B **38**, 1907–1922 (2005).
54. T. H. Yoon, A. Marian, J. L. Hall, and J. Ye, "Phase-coherent multilevel two-photon transitions in cold Rb atoms: Ultrahigh-resolution spectroscopy via frequency-stabilized femtosecond laser," Phys. Rev. A **63**, 011402(R) (2000).
55. A. Marian, M. C. Stowe, J. R. Lawall, D. Felinto, and J. Ye, "United time-frequency spectroscopy for dynamics and global structure," Science **306**, 2063–2068 (2004).
56. S. T. Cundiff and J. Ye, "Colloquium: Femtosecond optical frequency combs," Rev. Mod. Phys. **75**, 325–342 (2003).
57. B. Dubetsky and P. R. Berman, "Ground-state Ramsey fringes," Phys. Rev. A **56**, R1091–R1094 (1997).
58. M. Weel and A. Kumarakrishnan, "Observation of ground-state Ramsey fringes," Phys. Rev. A **67**, 061602(R) (2003).